

Chapter 10

Dynamical Processes in Globular Clusters

Stephen L. W. McMillan

10.1 Introduction

Globular clusters have long been regarded as near-perfect laboratories for studies of stellar physics and stellar dynamics. Some reasons (and complications) are:

- they are isolated in space (but not all clusters are found in galactic halos — many disk and bulge clusters are known, and dynamical friction has probably transported many clusters into the Galactic Centre)
- they contain coeval stars (but many clusters are now known to contain multiple stellar populations indicating several distinct phases of star formation)
- they contain virtually no gas or dust (today, that is — at early times, gas dynamical processes dominated their evolution)
- they are nearly spherical (although several are measurably flattened by rotation and/or tidal effects)

These systems thus represent a relatively — although not perfectly — “clean” realisation of the classical N -body problem

$$\mathbf{a}_i \equiv \ddot{\mathbf{x}}_i = \sum_{j \neq i}^N Gm_j \frac{\mathbf{x}_j - \mathbf{x}_i}{|\mathbf{x}_j - \mathbf{x}_i|^3}, \quad i = 1, \dots, N. \quad (10.1)$$

We begin our study of cluster dynamics by ignoring complicating factors such as gas dynamics, stellar evolution, mass loss, etc., and focus on the pure N -body problem, much as it might have been described by Newton. We define timescales and other units, discuss the fundamental dynamical processes driving cluster evolution, and present some basic terminology relevant to cluster dynamics.

Stephen McMillan
Department of Physics, Drexel University, Philadelphia, PA 19104, USA,
e-mail: steve@physics.drexel.edu

10.2 Virial Equilibrium

Star clusters have no static equilibrium configuration similar to that found in a fluid system such as a star. Stars are in constant motion. However, in dynamical equilibrium, at any given location in the cluster there are as many stars moving inward as moving outward — that is, there is no net radial stellar flux.

10.2.1 The Virial Theorem

A convenient global restatement of dynamical equilibrium involves the “radial moment of inertia” of the system

$$I = \sum_{i=1}^N m_i r_i^2, \quad (10.2)$$

where $r_i = |\mathbf{x}_i|$. Differentiating, we find

$$\dot{I} = 2 \sum_{i=1}^N m_i (v_i^2 + \mathbf{x}_i \cdot \mathbf{a}_i). \quad (10.3)$$

Setting $\dot{I} = 0$ as our definition of dynamical equilibrium, we have

$$\sum_{i=1}^N m_i v_i^2 + \sum_{i=1}^N m_i \mathbf{x}_i \cdot \mathbf{a}_i = 0. \quad (10.4)$$

The first term is simply twice the total kinetic energy of the system, $2K$. The second is easily shown to be

$$U = - \sum_{i=1}^N \sum_{j>i}^N \frac{Gm_i m_j}{|\mathbf{x}_j - \mathbf{x}_i|}, \quad (10.5)$$

the total potential energy of the system. Thus we obtain the (scalar) Virial Theorem

$$2K + U = 0. \quad (10.6)$$

If this relation holds the cluster is said to be in virial equilibrium. Since the total energy is $E = K + U$ (< 0), in virial equilibrium we have

$$K = -E, \quad U = 2E. \quad (10.7)$$

10.2.2 Length and Time Scales

We can define some characteristic physical scales for a system in virial equilibrium (Eq. 10.6). For a cluster of total mass M , the virial radius, R_{vir} , is defined as

$$R_{vir} \equiv -\frac{GM^2}{2U} = -\frac{GM^2}{4E}. \quad (10.8)$$

It defines a characteristic length scale for the cluster. It is typically comparable to the cluster half-mass radius, R_h , the radius of the sphere centred on the cluster enclosing half of the cluster's total mass. The two radii are often used interchangeably, although they are distinct physical quantities. Spitzer [119] notes that $R_{vir} \approx 0.8R_h$ for a broad range of common cluster models.

The cluster dynamical time (or “crossing time”), t_{dyn} , is

$$\begin{aligned} t_{dyn} &\equiv \left(\frac{GM}{R_{vir}^3}\right)^{-1/2} = \frac{GM^{5/2}}{(-4E)^{3/2}} \\ &= 0.47 \text{ Myr} \left(\frac{M}{10^6 \text{ M}_\odot}\right)^{-1/2} \left(\frac{R_{vir}}{10 \text{ pc}}\right)^{3/2}. \end{aligned} \quad (10.9)$$

The second forms of this and the previous expression conveniently define R_{vir} and t_{dyn} in terms of conserved quantities. The dynamical time is the characteristic orbital or free-fall time of a cluster. It is also the timescale on which an initially non-equilibrium cluster will establish virial equilibrium. Since t_{dyn} is generally short compared to all other dynamical timescales of interest, we assume virial equilibrium in all that follows.

Finally, the cluster-wide velocity dispersion $\langle v^2 \rangle$ is

$$\begin{aligned} \langle v^2 \rangle &= \frac{2K}{M} = \frac{GM}{2R_{vir}} \\ &= (14.7 \text{ km/s})^2 \left(\frac{M}{10^6 \text{ M}_\odot}\right) \left(\frac{R_{vir}}{10 \text{ pc}}\right)^{-1}. \end{aligned} \quad (10.10)$$

Dynamicists commonly write the total kinetic energy K in terms of the “thermodynamic” quantity kT , defined by

$$K = \frac{3}{2}NkT \quad (10.11)$$

so

$$kT = \frac{1}{3}\langle m \rangle \langle v^2 \rangle = -\frac{2E}{3N} \quad \text{in virial equilibrium,} \quad (10.12)$$

where $\langle m \rangle = M/N$ is the mean stellar mass.

Since gravity has no preferred scale, it is convenient to work in a system of dimensionless units such that all bulk cluster properties are of order unity. A system in widespread use, described in [65], has $G = 1$, $M = 1$, and $E = -\frac{1}{4}$, so $R_{vir} = 1$, $t_{dyn} = 1$, and $\langle v^2 \rangle = \frac{1}{2}$.

10.3 Relaxation

The long-term evolution of a star in hydrostatic equilibrium is driven by thermal and nuclear processes that transfer energy throughout the star and generate energy in the core. In a star cluster, thermal evolution is driven by two-body relaxation, while energy may be generated by a number of mechanisms, as discussed below.

To a first approximation (Fig. 10.1a), stars orbiting in a cluster move on relatively smooth orbits determined by the bulk mean-field gravitational potential of the system as a whole. However, stars occasionally experience close encounters with one another, changing their orbital parameters and transferring energy from one to the other (see Fig. 10.1b). This thermalising process allows energy to flow around the stellar system.

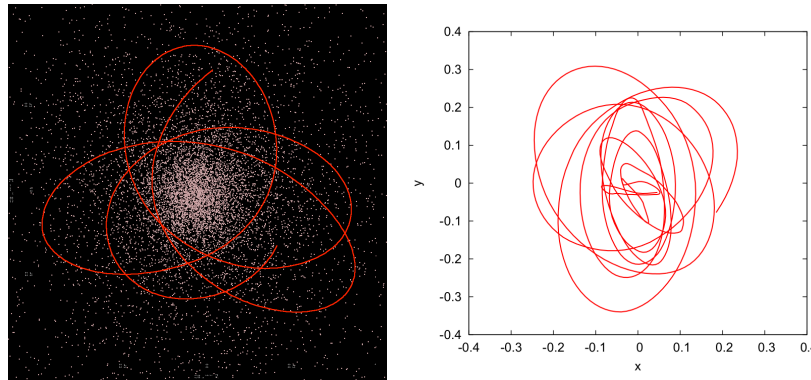


Fig. 10.1 (a) A typical smooth orbit in a 10,000-body system. The scale of this figure is ± 1 N -body units. (b) An orbit closer to the centre shows generally smooth behaviour, but also has a few sharp “kinks” associated with close encounters in the dense core.

10.3.1 Two-body Scattering

Our basic approximation here is the assumption that encounters between stars can be treated as isolated two-body scattering events. This is permissible because the scale of two-body encounters is generally much less than the scale of the system, so we can talk sensibly about stellar velocities at “infinity” in a scattering calculation without having to worry about the large-scale motion of stars around the cluster.

Imagine two stars of masses M_1 and M_2 approaching one another on unbound trajectories with relative velocity at infinity v_∞ and impact parameter b (Fig. 10.2). The solution for the relative orbit $\mathbf{r} = \mathbf{x}_1 - \mathbf{x}_2$ is

$$r(1 + e \cos \theta) = a(e^2 - 1),$$

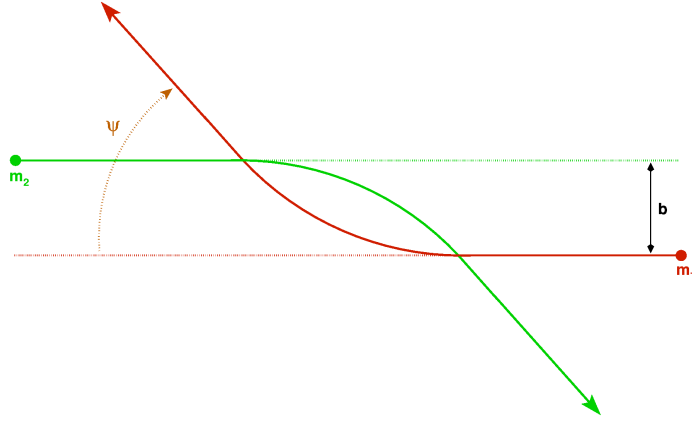


Fig. 10.2 Two stars, of masses M_1 and M_2 , approach one another with impact parameter b (and relative velocity at infinity v_∞), and are deflected by an angle ψ .

where (with $m = M_1 + M_2$), $a = Gm/v_\infty^2$ is the semi-major axis, and $e = \sqrt{1 + (bv_\infty/Gm)^2}$ is the eccentricity. The deflection angle is $\psi = \pi - 2\theta_1$, where

$$\tan \theta_1 = \frac{bv_\infty^2}{Gm}. \quad (10.13)$$

Thus the impact parameter corresponding to a 90° scattering, $\psi = \pi/2$ or $\theta_1 = \pi/4$, is

$$b_{90} = \frac{Gm}{v_\infty^2}. \quad (10.14)$$

More generally, for encounters in a cluster, we have $m \sim 2\langle m \rangle$ and $\langle v_\infty^2 \rangle \sim 2\langle v^2 \rangle$, and we may write

$$b_{90} \sim \frac{G\langle m \rangle}{\langle v^2 \rangle}. \quad (10.15)$$

For $\langle m \rangle \sim 1M_\odot$ and $\langle v^2 \rangle^{1/2} \sim 10$ km/s, Eq. (10.15) gives $b_{90} \sim 9$ AU. Combining Eqs. (10.10) and (10.15), we find $b_{90} \sim 2R_{\text{vir}}/N$.

10.3.2 Strong Encounters

The strong encounter timescale, t_s , is the time needed for a typical star to experience a 90° scattering. For a star of mass m_* moving with velocity v through a uniform field of identical stars with number density n , the cross section for a strong encounter is

$$\sigma = \pi b_{90}^2 = \frac{\pi G^2 m_*^2}{v^2}. \quad (10.16)$$

The timescale for a strong encounter is

$$t_s = (n\sigma v)^{-1} = \frac{v^3}{\pi G^2 m_*^2 n}. \quad (10.17)$$

Replacing m_* by the mean stellar mass $\langle m \rangle$, v^2 by the stellar velocity dispersion $\langle v^2 \rangle$, and writing $\langle m \rangle n = \rho$, we obtain

$$t_s = \frac{\langle v^2 \rangle^{3/2}}{\pi G^2 \langle m \rangle \rho}. \quad (10.18)$$

This is the relevant timescale for discussions of interactions involving close binaries (see §10.3.6.1 below).

10.3.3 Distant Encounters

The cross section for wide encounters, with smaller deflections $\psi \ll 1$, is much larger than that for a 90° scattering, but to estimate the cumulative effect of many small-angle deflections we must adopt a different approach. Consider again our star moving through a field of similar stars. For a single encounter with impact parameter b , the resulting velocity change transverse to the incoming velocity v may be shown to be (see, e.g., [14])

$$\delta v_\perp = 2v \left(\frac{b}{b_{90}} \right) \left(1 + \frac{b^2}{b_{90}^2} \right)^{-1}. \quad (10.19)$$

Integrating over repeated random encounters, we expect the mean velocity change in any direction transverse to the incoming velocity to be zero, by symmetry. However, the transverse velocity undergoes a symmetric, two-dimensional random walk, and we expect transverse velocity changes to add in quadrature, leading to a non-zero value for the mean square transverse velocity Δv_\perp^2 . During a time interval δt , the number of encounters with impact parameters in the range $[b, b + db)$ is $2\pi b db n v \delta t$, so integrating over all encounters, we find

$$\begin{aligned} \Delta v_\perp^2 &= 2\pi n v \delta t \int_0^{b_{max}} b db (\delta v_\perp)^2 \\ &\approx 8\pi \delta t \frac{G^2 m_*^2 n}{v} \ln \left(\frac{b_{max}}{b_{90}} \right), \end{aligned} \quad (10.20)$$

where we have assumed $b_{max} \sim R_{vir} \gg b_{90}$.

We can define a two-body relaxation timescale, δt_r , as the time interval in the above expression corresponding to $\Delta v_\perp^2 = v^2$. Rearranging the equation and replacing all quantities by mean values, as above, we find

$$\delta t_r = \frac{\langle v^2 \rangle^{3/2}}{8\pi G^2 \langle m \rangle \rho \ln \Lambda}, \quad (10.21)$$

where the “Coulomb logarithm” term (the term stemming from the almost identical development found in plasma physics) has $\Lambda = R_{\text{vir}}/b_{90} = \frac{1}{2}N$, from Eqs. (10.10) and (10.15).

There is considerable ambiguity in the above definition. For example, we could equally well have used Δv_{\parallel}^2 as our measure of relaxation, and our procedure neglects the distribution of relative velocities of stars in a real system. In fact, all approaches and refinements yield the same functional dependence on physical parameters as Eq. (10.21), but they differ in the numerical coefficient. The expression presented in [119], now widely adopted as a standard definition of the term, defines the relaxation time in terms of Δv_{\parallel}^2 , and averages over a thermal velocity distribution — the theoretical end point (not always realised in practice) of the relaxation process. The result is

$$\begin{aligned} t_r &= \frac{0.065 \langle v^2 \rangle^{3/2}}{G^2 \langle m \rangle \rho \ln \Lambda} \\ &= 3.4 \text{ Gyr} \left(\frac{\langle v^2 \rangle^{1/2}}{10 \text{ km/s}} \right)^3 \left(\frac{\langle m \rangle}{M_{\odot}} \right)^{-1} \left(\frac{\rho}{100 M_{\odot} \text{ pc}^{-3}} \right)^{-1} \left(\frac{\ln \Lambda}{10} \right)^{-1}. \end{aligned} \quad (10.22)$$

The precise definition of Λ is also the subject of a minor debate. Spitzer [119] chooses $b_{\text{max}} = R_h$ and hence writes $\Lambda = 0.4N$. Giersz & Heggie [51] calibrate the relaxation process using N -body simulations (see §10.5.3) and find $\Lambda \sim 0.1N$. For systems with a significant range of stellar masses, the effective value of Λ may be considerably smaller even than this value.

Although the analysis leading to Eq. (10.22) is global in nature, it is common to find this expression used as a *local* measure of the relaxation timescale in a system.

10.3.4 Comparison of Timescales

Comparing Eqs. (10.22) and (10.18), we see that

$$\frac{t_s}{t_r} \sim 5 \ln \Lambda \sim 60 \text{ for } N \sim 10^6,$$

so distant encounters dominate over close encounters in determining the flow of energy around the system.

Spitzer [119] defines a global relaxation timescale, often referred to as the *half-mass relaxation time*, t_{rh} , by replacing all quantities in Eq. (10.22) with their system-wide averages,

$$\begin{aligned}
\langle v^2 \rangle &\rightarrow \frac{GM}{2R_{vir}} \\
\rho &\rightarrow \frac{3M}{8\pi R_h^3} \\
\langle m \rangle &\rightarrow \frac{M}{N},
\end{aligned}$$

obtaining

$$\begin{aligned}
t_{rh} &= \frac{0.138NR_h^{3/2}}{G^{1/2}M^{1/2}\ln\Lambda} \\
&= 6.5 \text{ Gyr} \left(\frac{N}{10^6} \right) \left(\frac{M}{10^6 M_\odot} \right)^{-1/2} \left(\frac{R_h}{10 \text{ pc}} \right)^{3/2} \left(\frac{\ln\Lambda}{10} \right)^{-1}.
\end{aligned} \tag{10.23}$$

Hence, from Eqs. (10.9) and (10.23), we have

$$\frac{t_{rh}}{t_{dyn}} \sim \frac{N}{5\ln\Lambda}, \tag{10.24}$$

and we see that relaxation is a slow process relative to the dynamical time for all but the smallest systems.

We note in passing that the relaxation time (Eq. 10.22) evaluated at the half-mass radius R_h can differ significantly from the half-mass relaxation time (Eq. 10.23) — for example, for a $W_0 = 7$ King model, the former exceeds the latter by a factor of almost five — representing a potentially significant source of confusion in this terminology.

10.3.5 Cluster Dynamical Evolution

We can understand most aspects of the dynamical evolution of globular clusters in terms of the fundamental physics of self-gravitating systems just described.

10.3.5.1 Evaporation and Cluster Lifetimes

The relaxation time (Eq. 10.22) is the timescale on which stars tend to establish a Maxwellian velocity distribution. A fraction ξ_e of the stars in the tail of that distribution have velocities larger than v_{esc} and therefore escape. If this high-velocity tail is refilled every t_{rh} , then the dissolution time scale is $t_{dis} \sim t_{rh}/\xi_e$. For isolated clusters, $v_{esc} = 2\langle v^2 \rangle^{1/2}$ and $\xi_e = 0.0074$, implying $t_{dis} = 137t_{rh}$. For tidally limited clusters, ξ_e is higher since v_{esc} is lower. For a “typical” cluster density profile (with $R_h/RJ = 0.145$), Spitzer [119] finds $\xi_e \approx 0.045$, so $t_{dis} \approx 20t_{rh}$.

In fact, t_{dyn} also enters into the escape rate.

Baumgardt [7] found, for equal-mass stars, $t_{dis} \propto t_{rh}^{3/4} t_{dyn}^{1/4}$. This non-intuitive scaling of the dissolution time results from the fact that a star with sufficient energy to escape may orbit the system many times before finding one of the Lagrangian points, through which it eventually escapes [44].

Baumgardt & Makino [8] found that this non-linear scaling of the dissolution time with the relaxation time also holds for model clusters with a stellar mass spectrum, stellar evolution, and for different types of orbits in a logarithmic potential. Their result for t_{dis} may be summarised as

$$t_{dis} \approx 2 \text{ Myr} \left(\frac{N}{\ln \Lambda} \right)^{3/4} \left(\frac{R_G}{\text{kpc}} \right) \left(\frac{V_G}{220 \text{ km/s}} \right)^{-1} (1 - \varepsilon), \quad (10.25)$$

where ε is the ellipticity of the orbit. For non-circular orbits ($\varepsilon > 0$), the galactocentric distance R_G is taken as apogalacticon, while V_G is the circular velocity, which is constant in a logarithmic potential. Lamers, Gieles, & Portegies Zwart [84] found that, when the Coulomb logarithm is taken into account, the scaling is approximately $t_{dis} \propto N^{0.65}$ for $M \sim 10^3 - 10^6 M_\odot$.

The combined effects of mass loss by stellar evolution and dynamical evolution in the tidal field of the host galaxy have been extensively studied by a number of authors, including [19, 43, 129, 8, 136]. Mass loss due to stellar evolution, particularly during a cluster's early evolution (the first few hundred million years), can significantly reduce the cluster lifetime. Cluster expansion due to this mass loss can be substantial, and may even result in complete disruption if the cluster is mass segregated before the bulk of the stellar evolution takes place [134].

The expansion of a mass-segregated cluster will not be homologous, as the massive (segregated) core stellar population tends to lose relatively more mass than the lower-mass halo stars. The result is a more dramatic expansion of the cluster core, with less severe effects farther out. These above studies show that when clusters expand to a half-mass radius of $\sim 0.5 R_J$ they lose equilibrium and most of their stars overflow R_J in a few crossing times.

10.3.5.2 Core Collapse

The evaporation of high-velocity stars and the internal effects of two-body relaxation transfer energy from the inner to the outer regions of the cluster, resulting in the phenomenon of core collapse [3, 87, 21, 86, 88]. During this phase, the central portions of the cluster accelerate toward infinite density while the outer regions expand. The process is most easily understood by recognising that, according to the virial theorem (Eq. 10.7), a self-gravitating system has negative specific heat — reducing its energy causes it to heat up. Hence, as relaxation transports energy from the (dynamically) warmer central core to the cooler outer regions, the core contracts and heats up as it loses energy. The time scale for the process to go to completion (i.e. a core of zero size and formally infinite density) is $t_{cc} \sim 15 t_{rh}$ for an initial Plummer sphere of identical masses. Starting with a more concentrated King [81]

distribution shortens the time of core collapse considerably [115], as does a broad spectrum of masses [76].

In systems with a mass spectrum, the dynamical evolution is accelerated by the tendency of the system to evolve toward energy equipartition, in which the velocity dispersions of stars of different masses would have $\langle mv^2 \rangle \sim \text{constant}$. The result is mass segregation, where more massive stars slow down and sink toward the centre of the cluster on a timescale [120]

$$t_{\text{seg}} \sim \frac{\langle m \rangle}{m} t_{rh}. \quad (10.26)$$

Portegies Zwart & McMillan [106] and Gürkan, Freitag, & Rasio [59] find that, for a typical Kroupa [82] initial mass function, the timescale for the most massive stars to reach the centre and form a well defined high-density core is $\sim 0.2t_{rl}$, where t_{rl} is the relaxation time (Eq. 10.22) of the region containing a significant number of massive stars — the core of a massive cluster, or the half-mass radius of a smaller one (in which case $t_{rl} = t_{rh}$, see Eq. 10.23).

The post-collapse phase may involve a series of large-amplitude core oscillations, driven by the same basic instability as gravothermal collapse and involving the innermost few percent of the mass. First discovered in gas-sphere [13, 56] and later in Fokker–Planck [22] simulations (see §10.5), their existence in simple N -body systems was subsequently confirmed by Makino [88]. Like core collapse, these gravothermal oscillations appear to be a ubiquitous phenomenon. However, they are known to be suppressed by the presence of mass spectrum, as well as by primordial binaries and other heating mechanisms, and their reality in actual globular clusters remains unclear. However, significant core oscillations have been observed in realistic simulations of globular-cluster sized systems (Heggie 2012, private communication), and the effect of these substantial variations in central density may be important for the formation and subsequent evolution of exotica such as neutron star binaries and blue stragglers [58].

10.3.6 Internal Heating

On longer timescales, cluster evolution is driven by the competition between relaxation and a variety of internal heating mechanisms. High core densities lead to interactions among stars and binaries. Many of these interactions can act as energy sources to the cluster on larger scales, satisfying the relaxation-driven demands of the halo and temporarily stabilising the core against collapse [57, 47, 94, 95, 62, 37]. On long time scales, these processes lead to a relatively slow (relaxation time scale) overall expansion of the cluster, with $R_{\text{vir}} \propto t^{2/3}$, a result that follows from simple considerations of the energy flux through the half-mass radius [66].

10.3.6.1 Binary Interactions

Binaries in star clusters may be primordial (i.e. they were present when the cluster formed, or are descended from such systems), or they can form in a variety of ways, including dissipationless stellar-dynamical processes [119, 130] and dissipative processes such as tidal capture [35]. Regardless of how they formed, binaries are described by dynamicists as either “hard” or “soft,” depending on their binding energies. A hard binary has binding energy greater than the mean stellar kinetic energy in the cluster [61]: $|E_b| > \frac{1}{2} \langle mv^2 \rangle \approx \frac{1}{2} \langle m \rangle \langle v^2 \rangle$, where $\langle m \rangle$ and $\langle v^2 \rangle$ are the local mean stellar mass and velocity dispersion. A binary with mass $m_b = M_1 + M_2$ and semi-major axis a_b has energy $E_b = -GM_1M_2/2a_b$, so hard binaries have $a_b < a_{\text{hard}}$, where

$$a_{\text{hard}} = \frac{Gm_b^2}{4\langle m \rangle \langle v^2 \rangle} \approx 9.5 \times 10^4 R_\odot \left(\frac{m_b}{M_\odot} \right)^2 \left(\frac{\langle v^2 \rangle^{1/2}}{\text{km/s}} \right)^{-2}. \quad (10.27)$$

Here we have assumed that $M_1 = M_2 = \langle m \rangle$ in deriving the right-hand expression. The hard–soft distinction is often helpful when discussing dynamical interactions between binaries and other cluster members. However, since this definition of hardness depends on local cluster properties, the nomenclature changes with environment — a binary that is hard in the halo could be soft in the core.

The dynamical significance of hard binaries (see Eq. 10.27) has been understood since the 1970s [61, 68, 73]. When a hard binary interacts with another cluster star, the resultant binary (which may or may not have the same components as the original binary) tends, on average, to be harder than the original binary, making binary interactions a net heat source to the cluster. Soft binaries tend to be destroyed by encounters. For equal-mass systems, the mean energy liberated in a hard-binary encounter is proportional to E_b : $\langle \Delta E_b \rangle = \gamma E_b$, where $\gamma = 0.4$ for “resonant” interactions [61], and $\gamma \sim 0.2$ when wider “flybys” are taken into account [119].

The liberated energy goes into the recoil of the binary and single star after the interaction. Writing the binary energy as $E_b = -hkT$ (see §10.2.2), where $h \gg 1$, the total recoil energy, in the centre of mass frame of the interaction, is γhkT . A fraction $\frac{m_b}{m_b+m}$ of this energy goes to the single star (of mass m) and $\frac{m}{m_b+m}$ to the binary. For equal-mass stars, these fractions reduce to $\frac{2}{3}$ for the single star and $\frac{1}{3}$ for the binary. Neglecting the thermal motion of the centre of mass frame, we can identify three regimes:

1. If $\frac{2}{3} \gamma hkT < \frac{1}{2} mv_{\text{esc}}^2 = 2m \langle v^2 \rangle = 6kT$, i.e. $h < 45$, neither the binary nor the single star acquires enough energy to escape the cluster. Binaries in this stage are kicked out of the core, then sink back by dynamical friction.
2. If $\frac{2}{3} \gamma hkT > 6kT$ but $\frac{1}{3} \gamma hkT < 4m \langle v^2 \rangle = 12kT$, i.e. $45 < h < 180$, the single star escapes, but the binary is retained.
3. If $h > 36/\gamma = 180$, both the binary and the single star are ejected.

These numbers are valid only for equal-mass stars, and are intended for illustration only. For a binary with components more massive than average, as is often the case, the threshold for single star ejection drops, while that for self-ejection increases.

The binary encounter timescale is $t_{enc} = (n\sigma\langle v^2 \rangle)^{-1}$, where n is the local stellar density and σ is the encounter cross section (see Eq. 10.30). If we arbitrarily compute the binary interaction cross section as that for a flyby within 3 binary semi-major axes, consistent with the encounters contributing to the Spitzer [119] value $\gamma = 0.2$, and again assume equal masses ($m_b = 2m$), we find

$$t_{enc} \sim 8ht_r, \quad (10.28)$$

where we have used Eq. (10.22) and taken $\ln \Lambda = 10$. Thus the net local heating rate per binary during the 100% efficient phase (#1 above), when the recoil energy remains in the cluster, is

$$\gamma h k T t_{enc}^{-1} \sim 0.1 k T / t_r, \quad (10.29)$$

that is, on average, each binary heats the cluster at a roughly constant rate. During phase 2, the heating rate drops to just over one-third of this value. The limiting value of one-third is not reached since the ejected single stars still heat the cluster indirectly by reducing its binding energy by a few kT . For “self-ejecting” binaries, the heating rate drops almost to zero, with only indirect heating contributing.

Binary–binary interactions also heat the cluster, although the extra degrees of freedom complicate somewhat the above discussion. If the binaries differ widely in semi-major axes, the interaction can be handled in the three-body approximation, with the harder binary considered a point mass. If the semi-major axes are more comparable, as a rule of thumb the harder binary tends to disrupt the wider one [4].

Numerical experiments over the past three decades have unambiguously shown how initial binaries segregate to the cluster core, interact, and support the core against further collapse [94, 62]. The respite is only temporary, however. Sufficiently hard binaries are ejected from the cluster by the recoil from their last interaction, and binaries may be destroyed by interactions with harder binaries, or by collisions during the interaction. For large initial binary fractions, this binary-supported phase may exceed the age of the universe or the lifetime of the cluster against tidal dissolution. However, for low initial binary fractions, as appears to have been the case for the globular clusters observed today [97], the binaries can be depleted before the cluster dissolves, and core collapse resumes [37].

10.3.6.2 Stellar Collisions

In systems without significant binary fractions — either initially or following the depletion of core binaries — core collapse may continue to densities at which actual stellar collisions occur. In young clusters, the density increase may be enhanced by rapid segregation of the most massive stars in the system to the cluster core. Since the escape velocity from the stellar surface greatly exceeds the *rms* speed of cluster stars, collisions are expected to lead to mergers of the stars involved, with only

small fractional mass loss [11, 39]. If the merger products did not evolve, the effect of collisions would be to dissipate kinetic energy, and hence cool the system, accelerating core collapse [109]. However, when accelerated stellar evolution is taken into account, the (time averaged) enhanced mass loss can result in a net heating effect [18].

The cross section for an encounter between two objects of masses M_1 and M_2 and radii r_1 and r_2 , respectively, is [69]

$$\sigma = \pi r^2 \left[1 + \frac{2Gm}{rv^2} \right], \quad (10.30)$$

where v is the relative velocity at infinity, $m = M_1 + M_2$, and $r = r_1 + r_2$. For $r \ll Gm/v^2$, as is usually the case for the objects of interest here, the encounter is dominated by the second term (gravitational focusing), and Eq. (10.30) reduces to

$$\sigma \approx 2\pi r \frac{Gm}{v^2}. \quad (10.31)$$

Collisions between unbound single stars are unlikely unless one or both of the stars is very large and/or very massive, or the local density is very high. However, the presence of a substantial binary population can significantly increase the chance of a stellar collision. The closest approach between particles in a resonant interaction may be as little as a few percent of the binary semi-major axis [74], so the hardest binaries may well experience physical stellar collisions rather than hardening to the point of ejection. It is quite likely that the third star will also be engulfed in the collision product [38]. Alternatively, before its next interaction, the binary may enter the regime in which internal processes, such as tidal circularisation and/or Roche lobe overflow, become important. The future of such a binary may be determined by the internal evolution of its component stars, rather than by further encounters.

Since binaries generally have semi-major axes much greater than the radii of the component stars, these binary-mediated collisions play important roles in determining the stellar collision rate in most clusters [106], leading to significant numbers of mergers in lower-density, binary rich environments. Massive binaries in dense clusters tend to be collision targets rather than heat sources [59].

10.4 Multiple Stellar Populations

The discovery of multiple populations of main-sequence stars and giants in an increasing number of globular clusters [103, 104] has led to the realisation that these clusters are not idealised entities with single well defined stellar populations. In many systems the observed stellar populations appear to be separated by less than $\sim 10^8$ years. The existence of multiple populations suggests that a second epoch of star formation must have taken place early in the cluster's lifetime. The differences in light-element abundances suggest that the second-generation (SG) stars formed

out of gas containing matter processed through high-temperature CNO cycle reactions in first-generation (FG) stars [16, 17].

The origin of the gas from which SG stars form is still an open question. Current leading models involve AGB stars [23, 78], rapidly rotating massive stars [114, 27], and massive binaries ([26], see also [116] for a review). In order to explain the observed abundance patterns, all current models require that “pristine” (i.e. unprocessed) gas must be included in the SG mix (see [25] and references therein). In addition, in order to form the numbers of SG stars observed today, the FG cluster must have been considerably more massive than it is now, and the majority of stars in the cluster initially belonged to the FG population.

Many fundamental questions concerning globular cluster star formation and cluster chemical and dynamical history are raised by the discovery of multiple populations, and they have been targets of numerous theoretical investigations [24, 25, 9, 132]. Recently, Bastian et al. [6] have described a scenario that avoids both the mass problem and the need for multiple star-formation episodes by considering the accretion of CNO enriched material onto still-forming protostellar discs.

In many cases, the models suggest that the SG (“enriched”) population should initially be significantly more centrally concentrated than the FG stars. Decressin et al. [28] and Vesperini et al. [133] have studied the subsequent evolution and mixing of the two-component cluster in the first scenario. Vesperini et al. [133] find that the timescale for complete mixing depends on the SG initial concentration, but in all cases complete mixing is expected only for clusters in advanced evolutionary phases, having lost at least 60–70 percent of their mass due to two-body relaxation. These scenarios may be relevant to the properties of blue stragglers because they suggest that the FG and SG binary populations should have significantly different dynamical histories, with the SG binaries having spent much of their lives in much denser environments. One might naively expect these differences to manifest themselves in the properties of FG and SG blue stragglers, although the limited data currently available give little hint of any such effect (see Chap. 5).

10.5 Modeling Star Clusters

Although the fundamental physics is not hard to understand, simulating star clusters can be a complex numerical undertaking. Significant complications arise due to the long-range nature of the gravitational force, which means that every star in the cluster is effectively in constant communication with every other, leading to high computational cost. Further complications arise from the enormous range in spatial and temporal scales inherent in a star cluster. Computers, by the way they are constructed, have difficulty in resolving such wide ranges, and many of the software problems in simulations of self-gravitating systems arise from this basic limitation. The combination of many physical processes occurring on many scales, with high raw processing requirements, makes numerical gravitational dynamics among the

most demanding and challenging areas of computational science. Here we discuss some issues involved in the numerical modeling of massive star clusters.

A broad spectrum of numerical methodologies is available for simulating the dynamical evolution of globular clusters. In approximate order of increasing algorithmic and physical complexity, but not necessarily in increasing numerical complexity, the various methods may be summarised as follows.

- *Static Models* are self-consistent potential–density pairs for specific choices of phase-space distribution functions [105, 81, 14]. They have been instrumental in furthering our understanding of cluster structure, and provide a framework for semi-analytical treatments of cluster dynamics. However, they do not lend themselves to detailed study of star cluster evolution, and we will not discuss them further here.
- “*Continuum*” *Models* treat the cluster as a quasi-static continuous fluid whose phase-space distribution function evolves under the influence of two-body relaxation and other energy sources (such as binary heating) that operate on relaxation timescales (Eq. 10.23).
- *Monte Carlo Models* treat some or all components of the cluster as pseudo-particles whose statistical properties represent the continuum properties of the system, and whose randomly chosen interactions model relaxation and other processes driving the long-term evolution.
- *Direct N-body Models* follow the individual orbits of all stars in the system, automatically including dynamical and relaxation processes, and modeling other physical processes on a star-by-star basis.

Much of our current understanding of the evolution of star clusters comes from detailed numerical simulations, and the above techniques are used for the vast majority of simulations. Here we present a few details of these simulation techniques. We end with brief discussions of new computer hardware and the state of the art in modern simulation codes.

10.5.1 Continuum Methods

The two leading classes of continuum models are gas-sphere [86, 13, 30] and Fokker–Planck [20, 117, 19, 31, 126, 127, 128] methods. They have mainly been applied to spherically symmetric systems, although axisymmetric extensions to rotating systems have also been implemented [34, 79, 80], and a few limited experiments with simplified binary treatments have also been carried out [47].

Both approaches start from the collisional Boltzmann equation as the basic description for a stellar system, then simplify it by averaging the distribution function $f(\mathbf{x}, \mathbf{v})$ in different ways. Gas-sphere methods proceed in a manner analogous to the derivation of the equations of fluid motion, taking velocity averages to construct the moments of the distribution: $\rho = \int d^3v f(\mathbf{x}, \mathbf{v})$, $\mathbf{u} = \int d^3v \mathbf{v} f(\mathbf{x}, \mathbf{v})$, $\sigma^2 = \frac{1}{3} \int d^3v v^2 f(\mathbf{x}, \mathbf{v})$, etc. Application of an appropriate closure condition leads

to a set of equations identical to those of a classical conducting fluid, in which the conductivity depends inversely on the local relaxation time. Fokker–Planck methods transform the Boltzmann equation by orbit-averaging all quantities and recasting the equation as a diffusion equation in $E - J$ space, where E is stellar energy and J is angular momentum. Since both E and J are conserved orbital quantities in a static, spherically symmetric system, two-body relaxation enters into the problem via the diffusion coefficients.

These methods have been of enormous value in developing and refining theoretical insights into the fundamental physical processes driving the dynamical evolution of stellar systems [13]. However, as the degree of realism demanded of the simulation increases — adding a mass spectrum, stellar evolution, binaries, etc. — the algorithms rapidly become cumbersome, inefficient, and of questionable validity [107].

10.5.2 Monte Carlo Methods

Depending on one’s point of view, Monte Carlo methods can be regarded as particle algorithms for solving the partial differential equations arising from the continuum models, or approximate schemes for determining the long-term average gravitational interactions of a large collection of particles. The early techniques developed in the 1970s and 1980s [121, 67, 118, 124, 125] fall into the former category, but more recent studies [48, 77, 39, 49, 37, 50, 36, 63, 52, 53, 54], tend to adopt the latter view. The hybrid Monte Carlo scheme of [48, 49, 55] combines a gas-sphere treatment of the “background” stellar population with a Monte Carlo realisation of the orbits and interactions of binaries and other objects of interest. These approaches allowed the first simulations of an entire globular cluster, from a very early (although gas depleted) phase to complete dissolution.

Monte Carlo methods are designed for efficient computation of relaxation effects in collisional stellar systems, a task which they accomplish by reducing stellar orbits to their orbital elements — energy and angular momentum — effectively orbit averaging the motion of each star. Relaxation is modeled by randomly selecting pairs of stars and applying interactions between them in such a way that, on average, the correct rate is obtained. This may be implemented in a number of ways, but interactions are generally realised on timescales comparable to the orbit-averaged relaxation time. As a result, Monte Carlo schemes can be orders of magnitude faster than direct N -body codes. To achieve these speeds, however, the geometry of the system must be simple enough that the orbital integrals can be computed from a star’s instantaneous energy and angular momentum. In practice, this limits the approach to spherically symmetric systems in virial equilibrium, and global dynamical processes occurring on relaxation (or longer) timescales.

10.5.3 *N-body Methods*

N -body codes incorporate detailed descriptions of stellar dynamics at all levels, using direct integration of the individual (Newtonian) stellar equations of motion for all stars [1, 64]. Their major attraction is that they are assumption-free, in the sense that all stellar interactions are automatically included to all orders, without the need for any simplifying approximations or the inclusion of additional reaction rates to model particular physical processes of interest. Thus, problems inherent to Fokker–Planck and Monte Carlo methods related to departures from virial equilibrium, spherical symmetry, statistical fluctuations, the form of (and indeed the existence of) phase space distribution functions, and the possibility of interactions not explicitly coded in advance, simply do not arise, and therefore do not require fine-tuning as in the Monte Carlo models.

The price of these advantages is computational expense. Each of the N particles must interact with every other particle a few hundred times over the course of every orbit, each interaction requires $O(N)$ force calculations, and a typical (relaxation time) run spans $O(N)$ orbits (see Eq. 10.24). The resulting $O(N^3)$ scaling of the total CPU time means that, even with the best time-step algorithms, integrating even a fairly small system of a few hundred thousand stars requires sustained teraflops speeds for several months [75]. Radically improved performance can be achieved by writing better software, or by building faster computers (or both). However, the remarkable speed-up of N -body codes over the last four decades has been due mainly to advances in hardware.

Substantial performance improvements were realised by adopting better (individual) time stepping schemes (as opposed to earlier shared time step schemes), in which particles advance using steps appropriate to their individual orbits, rather than a single step for all. Block time step schemes [92, 91] offer still better performance. Further gains were made by utilising neighbour schemes [2], which divide the force on every particle into irregular (rapidly varying) and regular (slowly varying) parts, due (loosely speaking) to nearby and more distant bodies. By recomputing the regular force at every particle step, but extrapolating the more expensive $O(N)$ regular force for most time steps, and recomputing it only on longer timescales, significant improvements in efficiency are realised. These schemes form the algorithmic basis for Aarseth’s NBODY6 [1] and its parallel counterpart NBODY6++ [122].

The 1980s saw a major algorithmic improvement with the development of tree codes [5], which reduce the force calculation complexity from $O(N)$ to $O(\log N)$. However, despite their algorithmic efficiency, tree codes have not been widely used in modeling collisional systems (but see [93]). This may be due to lingering technical concerns about their long-term accuracy in systems dominated by relaxation processes and their performance in clusters with large dynamic ranges in densities and timescales, even though these objections may not be well founded [98, 29].

In recent years, meta-algorithms have been developed that enable straightforward combination of previously distinct dynamical algorithms to address new, more complex simulations. The first application of this approach permitted detailed study of the interaction between a star cluster (modeled by a direct N -body) and the

surrounding galactic stellar population (modeled by a tree code) [42, 111]. This “bridge” scheme has subsequently been generalised [101, 102] to couple arbitrary dynamical integration schemes, and now allows stellar- and gas-dynamical codes to be combined in ways that were previously impossible to realise.

10.5.4 Hardware Acceleration

The “GRAPE” (short for “GRAVity Pipe”) series of machines developed by Sugimoto and co-workers at Tokyo University [32], represented a quantum leap in gravitational N -body simulation speed. Abandoning algorithmic sophistication in favour of simplicity and raw computing power, GRAPE systems achieved high performance by mating a fourth-order Hermite integration scheme [90] with special-purpose hardware in the form of highly parallel, pipelined accelerators implementing the computation of all inter-particle forces entirely in hardware. Operationally, the GRAPE hardware was simple to program, as it merely replaced the function that computes the force on a particle by a call to hardware interface libraries, leaving the remainder of the user’s N -body code unchanged.

In recent years, as in many specialty fields, the market appears to have overtaken niche hardware solutions, and *Graphics Processing Units* (GPUs) have largely replaced GRAPEs in most N -body codes. GPU accelerated codes now surpass the older GRAPE benchmarks for raw performance and price/performance by a substantial margin. Fortunately, the GRAPE-accelerated code has not been discarded, as GPUs can serve as very efficient GRAPE emulators (see [112, 60, 10, 45] for various GPU implementations of the GRAPE interface). Besides GRAPE emulation, however, the much more flexible programming model for GPUs (as well as the GRAPE-DR [89]), means that many other kinds of algorithms can (in principle) be accelerated, although, in practice, it currently seems that CPU-intensive operations such as direct N -body force summation show substantially better acceleration than, say, tree codes running on the same hardware.

Today, GPU-enabled code lies at the heart of almost all detailed N -body simulations of star clusters and dense stellar systems. The GPU accelerated NBODY6-GPU [100] represents the current state of the art in raw N -body speed on workstations, and numerous parallel, GPU-accelerated N -body codes now exist or are under development, including HiGPUs [15], phiGPU [12], ph4 [96], and NBODY6++ [122, 123, 135] GPU accelerated versions of sixth and eighth order extensions of the standard fourth-order Hermite scheme [99], with and without neighbour schemes, are also becoming widespread.

10.5.5 The Kitchen Sink

The leading simulation programs in this field are “kitchen sink” packages that combine treatments of dynamics, stellar and binary evolution, and stellar hydrodynamics within a single simulation. Of these, the most widely used are the N -body codes NBODY [71, 1], (Hurley et al. 2001, Aarseth 2003), KIRA which is part of the STARLAB package (e.g. [110]), the MOCCA Monte Carlo code developed by Giersz and collaborators [48, 63, 52, 54], and the Northwestern MC Monte Carlo code [37, 41, 36].

Despite the differences in their handling of the large-scale dynamics, these codes all employ similar approaches to stellar and binary evolution and collisions. All use approximate descriptions of stellar evolution, generally derived from look-up tables based on the detailed evolutionary models of [33] and [70]. They also rely on semi-analytic or heuristic rule-based treatments of binary evolution [108, 72], conceptually similar from code to code, although significantly different in detail and implementation.

In most cases, stellar collisions are implemented in the “sticky-sphere” approximation, where stars are taken to collide (and merge) if they approach within the sum of their effective radii. The radii are calibrated using hydrodynamical simulations, and in some cases mass loss is included in an approximate way. Freitag’s Monte Carlo code, geared mainly to studies of galactic nuclei, interpolates encounter outcomes from a pre-computed grid of smoothed Particle Hydrodynamics (SPH) simulations [40]. Interesting alternatives, currently only operational in AMUSE (see below), are the “Make Me A Star” package (MMAS; [85]) and its extension “Make Me a Massive Star” (MMAMS; [46]). They construct a merged stellar model by sorting the fluid elements of the original stars by entropy or density, then recomputing their equilibrium configuration, using mass loss and shock heating data derived from SPH calculations.

Small-scale dynamics of multiple stellar encounters, such as binary and higher-order encounters, are often handled by look-up from pre-computed cross sections or — more commonly — by direct integration, either in isolation or as part of a larger N -body calculation. Codes employing direct integration may also include post-Newtonian terms in the interactions between compact objects [83].

10.5.6 The AMUSE Software Framework

The comprehensiveness of kitchen-sink codes gives them the great advantage of applicability to complex stellar systems, but also the significant disadvantage of inflexibility. By selecting such a code, one chooses a particular hard-coded combination of dynamical integrator, stellar and binary evolution schemes, collision prescription, and treatment of multiple dynamics. The structure of these codes is such that implementing a different algorithm within the larger framework is difficult at best for an expert, and impossible in practice for others.

AMUSE (the *Astrophysical Multipurpose Software Environment*) is a collaborative effort begun in 2008 designed to address this class of problem, providing a modular and extensible means of combining individual “monophysics” solvers into a unified astrophysical multiphysics simulation. The overarching goal of the project is to disentangle these components by providing a framework in which individual modules can interoperate, to facilitate experimentation and direct comparison of competing or alternative implementations of specific physical processes.

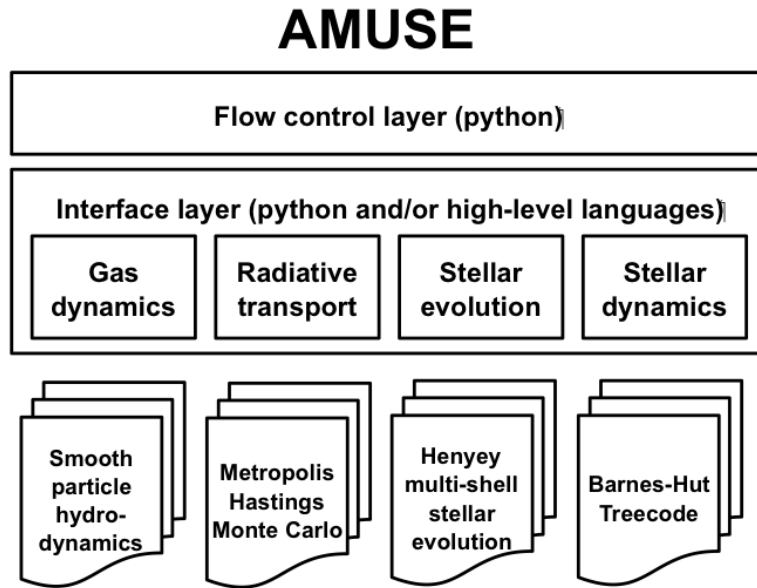


Fig. 10.3 The AMUSE environment. The top-level flow control layer is typically a custom GUI or user-written Python script that specifies the structure of the program, effectively replacing the top-level loop of a traditional program. Each of the four physics areas shown in the interface layer may be instantiated by one of several modules, allowing arbitrary combinations to be explored.

The global structure of AMUSE is illustrated in Fig. 10.3. In the AMUSE programming model, each piece of physics (advance the stellar or gas dynamics to a specified time, manage a close encounter, evolve a star, collide two stars, etc.) is implemented as a module with a standard interface onto the rest of the system, but the model details are private to each module. For example, all stellar modules include accessor functions that provide information on the mass and radius of a specified star, but the details of what a “star” actually is (an analytic formula, an entry in a look-up table, or a set of 1- or 2-D arrays describing the run of density, temperature, composition, etc.) remain internal to the module and are normally invisible to the outside.

The high-level “glue” language for AMUSE is python, chosen for its rich feature set, ease of programming and rapid prototyping, object-oriented capabilities, large user base in the astronomical community, and extensive user-written software. The design of AMUSE places no restrictions on the choice of language for any given module.

In a typical application, the top-level loop (the flow control layer in Fig. 10.3) of a simulation is written entirely in python, allowing monitoring, analysis, graphics, grid management, and other tools to be employed. The relatively low speed of the language does not significantly impact performance, because in practice virtually all of the computational load is carried by the (high-performance) physics modules.

Currently, AMUSE contains at least two (and typically more) independent modules for each physical process supported, allowing “plug and play” interchangeability between implementations. This modular approach enables, for the first time in this area of computational astrophysics, direct comparison and calibration of different implementations of the same physical processes, and facilitates experimentation in constructing new models. The integration of the parallel Message Passing Interface¹ (MPI) into AMUSE enables parallelism in all modules, allowing a serial user script to manage and transparently control modules that may themselves be parallel and/or GPU accelerated, possibly running on remote high-performance clusters.

Details on the structure and applications of AMUSE may be found on the project web site² and in [113, 102].

References

1. Aarseth, S. J.: *Gravitational N-Body Simulations*, Cambridge University Press (2003)
2. Ahmad, A., Cohen, L.: *J. Comp. Phys.* **12**, 289 (1973)
3. Antonov, V. A.: *Vestn. Leningr. Gos. Univ.* **7**, 135 (1962)
4. Bacon, D., Sigurdsson, S., Davies, M. B.: *MNRAS* **281**, 830 (1996)
5. Barnes, J., Hut, P.: *Nature* **324**, 446 (1986)
6. Bastian, N., Lamers, J. G. L. M., Longmore, S. N., Goodwin, S. P., de Mink, S., Gieles, M.: *MNRAS* **436**, 2398 (2013)
7. Baumgardt, H.: *MNRAS* **325**, 1323 (2001)
8. Baumgardt, H., Makino, J.: *MNRAS* **340**, 227 (2003)
9. Bekki, K.: *MNRAS* **412**, 2241 (2011)
10. Belleman, R. G., Bédorf, J., Portegies Zwart, S. F.: *New Astronomy* **13**, 103 (2008)
11. Benz, W., Hills, J. G.: *ApJ* **323**, 614 (1987)
12. Berczik, P., Nitadori, K., Zhong, S., et al.: in *Proc. 1st International Conference on High-Performance Computing, HPC-UA*, p.8 (2011)
13. Bettwieser, E., Sugimoto, D.: *MNRAS* **208**, 493 (1984)
14. Binney, J., Tremaine, S.: *Galactic Dynamics* (2nd Edition), Princeton University Press (2008)
15. Capuzzo-Dolcetta, R., Spera, M., Punzo, D.: *Journal of Computational Physics* **236**, 580 (2013)
16. Carretta, E., Bragaglia, A., Gratton, et al.: *A&A* **505**, 117 (2009a)
17. Carretta, E., Bragaglia, A., Gratton, R., Lucatello, S.: *A&A* **505**, 139 (2009b)

¹ <http://www.mcs.anl.gov/mpi>

² <http://amusecode.org>

18. Chatterjee, S., Fregeau, J. M., Rasio, F. A.: in *Dynamical Evolution of Dense Stellar Systems*, IAU Symp. 246, 151 (2008)
19. Chernoff, D. F., Weinberg, M. D.: *ApJ* **351**, 121 (1990)
20. Cohn, H.: *ApJ* **234**, 1036 (1979)
21. Cohn, H.: *ApJ* **242**, 765 (1980)
22. Cohn, H., Hut, P., Wise, M.: *ApJ* **342**, 814 (1989)
23. Cottrell, P. L., Da Costa, G. S.: *ApJ* **245**, L79 (1981)
24. D'Ercole, A., Vesperini, E., D'Antona, F., McMillan, S. L. W., Recchi, S.: *MNRAS* **391**, 825 (2008)
25. D'Ercole, A., D'Antona, F., Ventura, P., Vesperini, E., McMillan, S. L. W.: *MNRAS* **407**, 854 (2010)
26. de Mink, S. E., Pols, O. R., Langer, N., Izzard, R. G.: *A&A* **507**, L1 (2009)
27. Decressin, T., Meynet, G., Charbonnel, C., Prantzos, N., Ekström, S.: *A&A* **464**, 1029 (2007)
28. Decressin, T., Baumgardt, H., Kroupa, P.: *A&A* **492**, 101 (2008)
29. Dehnen, W.: *ApJL* **536**, L39 (2000)
30. Deiters, S., Spurzem, R.: *Astronomical and Astrophysical Transactions* **20**, 47 (2001)
31. Drukier, G. A., Fahlman, G. G., Richer, H. B.: *ApJ* **386**, 106 (1992)
32. Ebisuzaki, T., Makino, J., Fukushige, T., Taiji, M., Sugimoto D.: *PASJ* **45**, 269 (1993)
33. Eggleton, P. P., Fitchett, M. J., Tout, C. A.: *ApJ* **347**, 998 (1989)
34. Einsel, C., Spurzem, R.: *MNRAS* **302**, 81 (1999)
35. Fabian, A. C., Pringle, J. E., Rees, M. J.: *MNRAS* **172**, 15P (1975)
36. Fregeau, J. M., Rasio, F. A.: *ApJ* **658**, 1047 (2007)
37. Fregeau, J. M., Gürkan, M. A., Joshi, K.J., Rasio, F. A.: *ApJ* **593**, 772 (2003)
38. Fregeau, J. M., Cheung, P., Portegies Zwart, S. F., Rasio, F. A.: *MNRAS* **352**, 1 (2004)
39. Freitag, M., Benz, W.: *A&A* **375**, 711 (2001)
40. Freitag, M., Benz, W.: *MNRAS* **358**, 1133 (2005)
41. Freitag, M., Rasio, F. A., Baumgardt, H.: *MNRAS* **368**, 121 (2006)
42. Fujii, M., Iwasawa, M., Funato, Y., Makino, J.: *PASJ* **59**, 1095 (2007)
43. Fukushige, T., Heggie, D. C.: *MNRAS* **276**, 206 (1995)
44. Fukushige, T., Heggie, D. C.: *MNRAS* **318**, 753 (2000)
45. Gaburov, E., Harfst, S., Portegies Zwart, S. F.: *New Astronomy* **14**, 630 (2009)
46. Gaburov, E., Lombardi, J. C., Portegies Zwart S.: *MNRAS* **383**, L5 (2008)
47. Gao, B., Goodman, J., Cohn, H., Murphy, B.: *ApJ* **370**, 567 (1991)
48. Giersz, M.: *MNRAS* **298**, 1239 (1998)
49. Giersz, M.: *MNRAS* **324**, 218 (2001)
50. Giersz, M.: *MNRAS* **371**, 484 (2006)
51. Giersz, M., Heggie, D. C.: *MNRAS* **268**, 257 (1994)
52. Giersz, M., Heggie, D. C.: *MNRAS* **395**, 1173 (2009)
53. Giersz, M., Heggie D. C.: *MNRAS* **410**, 2698 (2011)
54. Giersz, M., Heggie, D.C., Hurley, J. R., Hypki, A.: *MNRAS* **431**, 2184 (2013)
55. Giersz, M., Spurzem, R.: *MNRAS* **343**, 781 (2003)
56. Goodman, J.: *ApJ* **313**, 576 (1987)
57. Goodman, J., Hut, P.: *Nature* **339**, 40 (1989)
58. Grindlay, J. E., Portegies Zwart, S. F. McMillan, S. L. W.: *Nature Physics* **2**, 116 (2006)
59. Gürkan, M. A., Freitag, M., Rasio, F. A.: *ApJ* **604**, 632 (2004)
60. Hamada, T., Iitaka, T.: *astro-ph/0703100* (2007)
61. Heggie, D. C.: *MNRAS* **173**, 729 (1975)
62. Heggie, D. C., Aarseth, S. J.: *MNRAS* **257**, 513 (1992)
63. Heggie, D. C., Giersz, M.: *MNRAS* **389**, 1858 (2008)
64. Heggie, D. C., Hut, P.: *The Gravitational Million-Body Problem: A Multidisciplinary Approach to Star Cluster Dynamics*, Cambridge University Press (2003)
65. Heggie, D. C., Mathieu R. D.: in *The Use of Supercomputers in Stellar Dynamics*, LNP Vol. 267, Springer-Verlag, p. 13 (1986)
66. Hénon, M.: *Annales d'Astrophysique* **28**, 62 (1965)

67. Hénon, M.: in Saas-Fee Advanced Course 3: Dynamical Structure and Evolution of Stellar Systems, Observatoire de Genève, p. 183 (1973)
68. Hills, J. G.: *AJ* **80**, 809 (1975)
69. Hills, J. G., Day, C. A.: *ApJL* **17**, 87 (1976)
70. Hurley, J. R., Pols, O. R., Tout, C. A.: *MNRAS* **315**, 543 (2000)
71. Hurley, J. R., Tout, C. A., Aarseth, S. J., Pols, O. R.: *MNRAS* **323**, 630 (2001)
72. Hurley, J. R., Tout, C. A., Pols, O. R.: *MNRAS* **329**, 897 (2002)
73. Hut, P., Bahcall, J. N.: *ApJ* **268**, 319 (1983)
74. Hut, P., Inagaki, S.: *ApJ* **298**, 502 (1985)
75. Hut, P., Makino, J., McMillan, S. L. W.: *Nature* **336**, 31 (1988)
76. Inagaki, S., Saslaw, W. C.: *ApJ* **292**, 339 (1985)
77. Joshi, K. J., Rasio, F. A., Portegies Zwart, S.: *ApJ* **540**, 969 (2000)
78. Karakas, A., Lattanzio, J. C.: *PASA* **24**, 103 (2007)
79. Kim, E., Einsel, C., Lee, H.-M., Spurzem, R., Lee, M. G.: *MNRAS* **334**, 310 (2002)
80. Kim, E., Lee, H.-M., Spurzem, R.: *MNRAS* **351**, 220 (2004)
81. King, I. R.: *AJ* **71**, 64 (1966)
82. Kroupa, P.: *MNRAS* **322**, 231 (2001)
83. Kupi, G., Amaro-Seoane, P., Spurzem, R.: *MNRAS* **371**, L45 (2006)
84. Lamers, H. J. G. L. M., Gieles, M., Portegies Zwart, S. F.: *A&A* **429**, 173 (2005)
85. Lombardi, J. C., Thrall, A. P., Deneva, J. S., Fleming, S. W., Grabowski P.E.: *MNRAS* **345**, 762 (2003)
86. Lynden-Bell, D., Eggleton, P. P.: *MNRAS* **191**, 483 (1980)
87. Lynden-Bell, D., Wood, R.: *MNRAS* **138**, 495 (1968)
88. Makino, J.: *ApJ* **471**, 796 (1996)
89. Makino, J.: *astro-ph/0509278* (2005)
90. Makino, J., Aarseth, S. J.: *PASJ* **44**, 141 (1992)
91. Makino, J., Hut, P., Kaplan, M., Saygin, H.: *New Astronomy* **12**, 124 (2006)
92. McMillan, S. L. W.: in *The Use of Supercomputers in Stellar Dynamics*, LNP Vol. 267, Springer-Verlag, p. 156 (1986)
93. McMillan, S. L. W., Aarseth, S. J.: *ApJ* **414**, 200 (1993)
94. McMillan, S. L. W., Hut, P., Makino, J.: *ApJ* **362**, 522 (1990)
95. McMillan, S. L. W., Hut, P., Makino, J.: *ApJ* **372**, 111 (1991)
96. McMillan, S., Portegies Zwart, S., van Elteren, A., Whitehead, A.: in *Advances in Computational Astrophysics: methods, tools and outcomes*, ASPC 435, p.129 (2012)
97. Milone, A. P., Piotto, G., Bedin, L. R., Sarajedini, A.: *MmSAI* **79**, 623 (2008)
98. Moore, B., Quinn, T., Governato, F., Stadel, J., Lake, G.: *MNRAS* **310**, 1147 (1999)
99. Nitadori, K., Makino, J.: *New Astronomy* **13**, 498 (2008)
100. Nitadori, K., Aarseth, S. J.: *MNRAS* **424**, 545 (2012)
101. Pelupessy, F. I., Portegies Zwart, S.: *MNRAS* **420**, 1503 (2012)
102. Pelupessy, F. I., van Elteren, A., de Vries, N., McMillan, S.L.W., Drost, N., Portegies Zwart, S.F.: *A&A* **557**, A84 (2013)
103. Piotto, G., Villanova, S., Bedin, L. R., Gratton, R., Cassisi, S., et al.: *ApJ* **621**, 777 (2005)
104. Piotto, G.: *MmSAI* **79**, 334 (2008)
105. Plummer, H. C.: *MNRAS* **71**, 460 (1911)
106. Portegies Zwart, S. F., McMillan, S. L. W.: *ApJ* **576**, 899 (2002)
107. Portegies Zwart, S. F., Takahashi, K.: *Celestial Mechanics and Dynamical Astronomy* **73**, 179 (1999)
108. Portegies Zwart, S. F., Verbunt, F.: *A&A* **309**, 179 (1996)
109. Portegies Zwart, S. F., Makino, J., McMillan, S. L. W., Hut, P.: *A&A* **348**, 117 (1999)
110. Portegies Zwart, S. F., McMillan, S. L. W., Hut, P., Makino, J.: *MNRAS* **321**, 199 (2001)
111. Portegies Zwart, S. F., McMillan, S. L. W., Harfst, S., Groen, D., Fujii, M., et al.: *New Astronomy* **14**, 369 (2009)
112. Portegies Zwart, S. F., Belleman, R. G., Geldof, P. M.: *New Astronomy* **12**, 641 (2007)
113. Portegies Zwart, S., McMillan, S. L. W., van Elteren, E., Pelupessy, I., de Vries, N.: *Computer Physics Communications* **184**, 456 (2013)

114. Prantzos, N., Charbonnel, C.: *A&A* **458**, 135 (2006)
115. Quinlan, G. D.: *New Astronomy* **1**, 255 (1996)
116. Renzini, A.: *MNRAS* **391**, 354 (2008)
117. Shapiro, S. L.: in *Dynamics of Star Clusters*, IAU Symp. 113, p. 373 (1985)
118. Spitzer, L.: in *Dynamics of the Solar Systems*, IAU Symp. 69, p. 3 (1975)
119. Spitzer, L.: *Dynamical evolution of globular clusters*, Princeton University Press (1987)
120. Spitzer, L. J.: *ApJL* **158**, 139 (1989)
121. Spitzer, L. J Hart, M. H.: *ApJ* **164**, 399 (1971)
122. Spurzem, R.: *Journal of Computational and Applied Mathematics* **109**, 407 (1999)
123. Spurzem, R., Berentzen, I., Berczik, P., Merritt, D., Amaro-Seoane, P., Harfst, S., Gualandris, A.: in *The Cambridge N-Body Lectures*, LNP Vol. 760, Springer-Verlag, p. 377 (2008)
124. Stodolkiewicz, J. S.: *Acta Astron.* **32**, 63 (1982)
125. Stodolkiewicz, J. S.: *Acta Astron.* **36**, 19 (1986)
126. Takahashi, K.: *PASJ* **48**, 691 (1996)
127. Takahashi, K.: *PASJ* **49**, 547 (1997)
128. Takahashi, K., Portegies Zwart, S. F.: *ApJL* **503**, 49 (1998)
129. Takahashi, K., Portegies Zwart, S. F.: *ApJ* **535**, 759 (2000)
130. Tanikawa, A., Hut, P., Makino, J.: *New Astronomy* **17**, 272 (2012)
131. Ventura, P., D'Antona, F., Mazzitelli, I., Gratton, R.: *ApJL* **550**, 65 (2001)
132. Vesperini, E., McMillan, S. L. W., D'Antona, F., D'Ercole, A.: *MNRAS* **416**, 355 (2011)
133. Vesperini, E., McMillan, S. L. W., D'Antona, F., D'Ercole, A.: *MNRAS* **429**, 1913 (2013)
134. Vesperini, E., McMillan, S. L. W., Portegies Zwart, S.: *ApJ* **698**, 615 (2009)
135. Wang, L., Nitadori, K., Spurzem, R., Berczik, P., Aarseth S.J.: in prep. (2014)
136. Whitehead, A., McMillan, S. L. W., Vesperini, E., Portegies Zwart, S.: *ApJ* **778**, 118 (2013)